RAA 2018 Vol. **18** No. **11**, 143(12pp) doi: 10.1088/1674–4527/18/11/143

http://www.raa-journal.org *http://iopscience.iop.org/raa*

***R**esearch in*
***A**stronomy and*
***A**strophysics*

Color gradients of the galaxies at $0.5 < z < 1$ I. Dependence on galaxy global properties

Zhi-Xiong Liang[1,2] and Cheng Li[3]

[1] Shanghai Astronomical Observatory, Chinese Academy of Sciences, Shanghai 200030, China; *zliang18@ustc.edu.cn*
[2] University of Chinese Academy of Sciences, Beijing 100049, China
[3] Tsinghua Center for Astrophysics and Physics Department, Tsinghua University, Beijing 100084, China

Received 2018 May 11; accepted 2018 May 21

Abstract We investigate the color gradients of galaxies at $0.5 < z < 1.0$, using a sample of ∼35 000 galaxies with both spectroscopy from the final data release of the VIMOS Public Extragalactic Redshift Survey (VIPERS), and photometry in ultraviolet/optical/near-infrared bands from the VIPERS-Multi-Lambda Survey (VIPERS-MLS) and the Canada-France-Hawaii Telescope Legacy Survey (CFHTLS). We estimate rest-frame colors, stellar mass, star formation rate from fitting the Spectral Energy Distribution (SED) for each galaxy, as well as a two-zone color $\Delta(u-r)$, defined as the difference in rest-frame $(u-r)$ color between the outer and inner region of the galaxy. We find that the two-zone color shows weak or no correlations with all galaxy properties considered except stellar mass. On average, $\Delta(u-r)$ decreases with increasing stellar mass, indicating relatively red colors in galactic centers of more massive galaxies. We then compare the properties of "red-cored" and "blue-cored" galaxies, defined to have either a negative or a positive $\Delta(u-r)$ respectively. Although the two types of galaxies show similar distributions in most properties, we find massive red-cored galaxies with $M_* > 10^{10.5}\,M_\odot$ to have larger sizes at given stellar mass (thus lower surface mass densities), and less massive red-cored galaxies with $M_* < 10^{10.5}\,M_\odot$ to have lower central galaxy fraction. These findings can be understood if one assumes that the star formation process happens from inside out, in the same way as recently emphasized in studies of low-z galaxies. The similarity between the galaxies at intermediate redshifts and those at low redshifts supports the idea that galaxy evolution since $z \sim 1$ has been mainly driven by secular processes internal to galaxies rather than galaxy mergers or external environment.

Key words: galaxies: photometry — galaxies: statistics — galaxies: evolution

1 INTRODUCTION

Radial color gradients or two zone colors of a galaxy are a combined effect of the radial variation of stellar population properties such as age, metallicity and dust attenuation. Therefore the radial color gradient of a galaxy, when combined with other physical properties, is expected to provide useful information about how the star formation history (SFH) varies across the galaxy. For instance, a significant fraction of massive galaxies is observed to be quiescent at $z \sim$1, but the physical processes responsible for rapid assembly of the quiescent population remain unclear. One may be able to discriminate between the processes by examining the color gradients, because different physical processes leave distinguishable imprints on the color gradients of massive quiescent galaxies (Guo et al. 2011). Wet major mergers (Daddi et al. 2005) or cool flows (Menanteau et al. 2001; Ferreras et al. 2005; Bildfell et al. 2008; Edwards et al. 2007; Wang et al. 2010) would form a blue core, while dry mergers would not.

For a large sample of galaxies with both imaging and spectroscopy available, the color gradient and other properties can be reliably measured and they combine to provide interesting constraints on the evolution processes of different galaxy populations. Earlier studies of

color gradients of galaxies revealed that most early-type galaxies (ETGs) have negative color gradients (i.e. redder in the inner region and bluer in the outer region), or flat color gradients (Boroson et al. 1983; Kormendy & Djorgovski 1989), which are believed to be driven by the metallicity gradient (Ferreras et al. 2009; Spolaor et al. 2010). Recent studies, however, have discovered a significant fraction of ETGs to present a positive color gradient (Menanteau et al. 2001; Ferreras et al. 2005; Suh et al. 2010), and these are attributed to gradients in both age and metallicity (Michard 2005).

The situation for late-type galaxies (LTGs) is more complex. Most LTGs also show negative color gradients (Kim & Ann 1990; de Jong 1996). Their redder cores are best explained by the younger age and lower metallicity in their outskirts, which cannot be caused by dust reddening alone at low-z. There is also quite a sizable fraction of LTGs showing positive or flat color gradients, especially at low masses (Kim & Ann 1990; Liu et al. 2009; Gonzalez-Perez et al. 2011; Cibinel et al. 2013). The physical process behind them remains unclear, however. Liu et al. (2016) found the star forming galaxies (SFGs) at $z \sim 1$ to generally present negative near-ultraviolet (NUV)–B color gradients. For low-mass SFGs, the negative gradient appeared to be caused by dust reddening in the central region of galaxies, but at high masses, the redder cores are likely a combined result of the central dust reddening together with the buildup of compact old bulges. At $z \sim 2$, dust reddening is likely the driving parameter for the redder cores in both low and high mass SFGs (Liu et al. 2017).

Most of our knowledge on color gradients has been obtained based on nearby galaxy samples, and galaxies at higher redshifts have not been extensively explored, mainly due to the lack of large galaxy samples at high redshifts. Up to now, studies of color gradients for intermediate or high redshift galaxies are limited to deep but narrow-area surveys carried out with space telescopes. Thanks to the VIMOS Public Extragalactic Redshift Survey (VIPERS)[1] and the Canada-France-Hawaii Telescope Legacy Survey (CFHTLS; Cuillandre et al. 2012)[2], both deep imaging in multiple bands and spectroscopy over large areas are available now for a large sample of galaxies at $0.5 < z < 1.2$, enabling us to investigate the color gradients and correlations with other properties for the galaxy population at $z \sim 1$, which is the cosmic epoch when the Universe was half of its current age and star formation activity was shutting down rapidly in galaxies.

In the next subsection, we will first give a brief introduction to the VIPERS and VIPERS-MLS data, as well as our methodology of measuring a variety of galaxy properties to be analyzed in this paper. In Section 3, we will then present our results. These include two parts: 1) the correlations of the two-zone color and color gradients of our galaxies with their global properties, and 2) comparisons of the galaxy properties for two subsets of galaxies with red or blue cores, which are selected according to the two-zone color of the galaxies. Finally, we summarize our work in Section 4.

Throughout this paper, we assume a flat ΛCDM cosmology with $\Omega_m = 0.3$ and $\Omega_\Lambda = 0.7$, and a Hubble constant of $H_0 = 70\,\mathrm{km\,s^{-1}\,Mpc^{-1}}$. All magnitudes are given in the AB system (Oke & Gunn 1983) and are corrected for Galactic extinction following Schlegel et al. (1998).

2 DATA

2.1 Sample

VIPERS[3] is a completed large redshift survey using the VIMOS spectrograph at the 8.2 m Very Large Telescope (Guzzo et al. 2014; Scodeggio et al. 2018). VIPERS obtained spectra for more than 90 000 galaxies with i-band AB magnitudes $i > 22.5$ and spectroscopic redshifts $0.5 < z < 1.2$. The galaxy targets were robustly selected based on color-color diagrams thanks to the multi-band deep imaging available in the same sky areas. VIPERS yields a high sampling rate of ∼50.1% and a success rate of reliable redshift measurements of ∼84.3%.

The footprint of VIPERS is separated into two regions, respectively falling within the W1 and W4 fields of the CFHTLS. The VIPERS fields are covered by a follow-up program, the VIPERS-Multi-Lambda Survey (VIPERS-MLS)[4] (Moutard et al. 2016a,b), which includes Ks-band photometry over $\sim 22\,\mathrm{deg}^2$ from WIRCAM and far-ultraviolet (FUV) and/or NUV photometry over $\sim 12.7\,\mathrm{deg}^2$ from *Galaxy Evolution Explorer* (*GALEX*; Martin et al. 2005), in addition to the five bands in the optical ($ugriz$) from CFHTLS. The u, g, r, i, z, Ks photometry produced by Terapix[5] was performed with SExtractor (Bertin & Arnouts 1996) in dual-image mode with the gri-χ^2 image as the detection image. The ultraviolet (UV) photometry was extracted

[1] *http://vipers.inaf.it*
[2] *http://www.cfht.hawaii.edu/Science/CFHTLS*
[3] *http://vipers.inaf.it/*
[4] *http://cesam.lam.fr/vipers-mls*
[5] *http://terapix.iap.fr*

from EMphot (Conseil et al. 2011), which takes u-band stamps as priors and the convolved (by the *GALEX* point spread function, PSF) ones as simulated images, deriving the scaling factor for each prior by maximizing the likelihood between observed and predicted fluxes simultaneously for all sources in each tile of several arcmin^2. The details of the VIPERS-MLS photometry process will be described in Vibert et al. (in prep.).

Both the VIPERS spectroscopic catalog and the VIPERS-MLS photometric catalog are publicly available. In this work we use data from both catalogs and we limit our analysis to a subset of galaxies with the following restrictions:

$$\begin{cases} 2.0 < z_{\rm flg} < 10 \\ R50 > 0.55\,{\rm PSF}_{\rm fwhm} \\ 0.5 < z < 1 \\ b/a > 0.5 \end{cases} , \quad (1)$$

where $z_{\rm flg}$ is the redshift flag denoting the quality of the redshift measurement, $R50$ is the radius of a galaxy enclosing half of its total light in the i-band, ${\rm PSF}_{\rm fwhm}$ is the full-width at half maximum of the PSF and b/a is the minor-to-major axis ratio measured from the i-band image. The first criterion on $z_{\rm flg}$ aims to keep only the high-quality redshift measurements. The reason for the requirements in both $R50$ and b/a is to have substantially high spatial resolution, so that we can reliably measure the color gradient of our galaxies. We exclude the galaxies at $z > 1$ both because the sample completeness drops quickly at the highest redshifts and because the galaxies become too small to allow measurements of color gradients.

These restrictions give rise to a sample of 35 279 galaxies, distributed over a total area of 23.5 deg^2. The effective area is reduced to 16.3 deg^2 after the photometric and spectroscopic selections are considered. Since the FUV/NUV photometry is available only for ∼50% of the survey area, about half of our galaxies have photometry in all the bands including FUV/NUV, u, g, r, i, z and Ks, while the other ∼40% of galaxies have u, g, r, i, z and Ks only.

The criterion of $R50 > 0.55\,{\rm PSF}_{\rm fwhm}$ corresponds to a Gaussian profile source being resolved at the minimum level. A stricter requirement of $R50 > {\rm PSF}_{\rm fwhm}$ leads to a sample of 9087 galaxies. In this work we will use the larger sample (hereafter `Sample S0.55`) as our main sample, and use the smaller one (hereafter `Sample S1.0`) as a comparison sample.

2.2 SED Fitting

We have performed Spectral Energy Distribution (SED)-fitting to the SED of each of our galaxies, from UV to near-infrared (NIR) (FUV, NUV, u, g, r, i, z and Ks), using the public code CIGALE[6] (Noll et al. 2009). The SED-fitting is done both for the whole galaxy, and for the inner and outer regions separately in order to estimate the color gradients. CIGALE includes stellar synthesis models as well as dust emission templates to allow for estimation of a series of physical properties and the best computed model by means of a Bayesian-like statistical analysis. For this work we focus on the derived star formation rate (SFR), stellar mass (M_*), infrared (IR) luminosity and rest-frame colors. In the fitting, we have adopted the BC03 stellar population synthesis model (Bruzual & Charlot 2003), the Salpeter stellar initial mass function (IMF; Salpeter 1955), the dust absorption law according to Calzetti et al. (2000), the dust emission model according to Dale et al. (2014) and the SFH described by a double exponentially decreasing SFR (Maraston et al. 2010; Papovich et al. 2011). The overall contribution of an active galactic nucleus (AGN) to the total IR luminosity is set to zero in our fitting because we have excluded AGNs by requiring $z_{\rm flg} < 10$. The CIGALE parameters are summarized in Table 1.

2.3 Color Gradients and Galaxy Classifications

The spatial resolution of the CFHTLS-wide images allows us to probe the color gradient in our galaxies. The half-light radius ($R50$) is comparable to, or even smaller than, the PSF of the images (${\rm PSF}_{\rm fwhm}$) for most of our galaxies (see the right-hand panel of Fig.1). This means we are allowed to independently measure colors only in two or three radial bins within a given galaxy. Therefore, we choose to measure the colors only in two regions: an inner region and an outer region, defined as the regions enclosed by $R < R20$ and $R50 < R < R80$ respectively. Here, $R20$, $R50$ and $R80$ are the radii enclosing $20\%, 50\%$ and 80% of the total light respectively, as measured from the convolved i-band images. We derive the broad-band SED of both the inner and outer regions, and perform SED fitting for the two regions separately. This results in the rest-frame magnitudes, k-corrected to the rest-frame from the SED fitting, from which we define a two-zone color as

$$\Delta(u-r) = (u-r)_{\rm outer} - (u-r)_{\rm inner} , \quad (2)$$

[6] *https://cigale.lam.fr/*

Table 1 CIGALE Parameters

Parameter descriptions	Parameter values
E-folding time of the old population	0.25, 0.5, 1.0, 1.5, 2.5, 4, 6, 8, 10 Gyr
Variable e-folding time of the late starburst population	10, 25, 50, 100, 200, 350, 500, 800 Myr
Mass fraction of the late burst population	0.001, 0.02, 0.06, 0.2, 0.4 , 0.8
Age of the late burst	5, 10, 25, 50, 100, 200, 300, 400, 500 Myr
Metallicity	0.004, 0.008, 0.02, 0.05
$E(B-V)$ of the stellar continuum light for the young population	0.01, 0.1, 0.2, 0.4, 0.6, 0.8 mag
Amplitude of the UV bump	0, 1, 2, 3
Slope δ of the power law modifying the attenuation curve	0.0
AGN fraction	0.0
Reduction factor for the $E(B-V)$ of the old population	0.44
IMF	Salpeter
Ionization parameter	10^{-2}
Fraction of Lyman continuum photons escaping the galaxy	0.0%
Fraction of Lyman continuum photons absorbed by dust	10%

and a color gradient as

$$G_{\rm ur} = \frac{\Delta(u-r)}{0.5(R50+R80)} \quad . \tag{3}$$

We classify each galaxy as star-forming or passive on the diagram of rest-frame NUV $-$ r vs. $r-Ks$ (NUVrK), following the classification criterion of Ilbert et al. (2015), which is an improved version of the criterion of Arnouts et al. (2013). Galaxies with $(\mathrm{NUV}-r)+C<2.6$ and $(\mathrm{NUV}-r)+C<2(r-K)+1.7$ are classified as SFGs, where C is a correction factor depending on the age of the Universe (t_H) at redshift z: $C=-0.17[t_H(z)-t_H(z=2)]$. Adding this factor makes the dividing cut universal to different redshifts (Ilbert et al. 2015).

In addition, we identify the "central" galaxies in our sample. A galaxy is defined as a central galaxy if it is locally dominating, that is, it is the most massive galaxy over a local cylindrical volume with a projected radius of $3\,h^{-1}$ Mpc and a line-of-sight depth of $1000\,\mathrm{km\,s^{-1}}$. Out of the 35 279 galaxies in `Sample S0.55`, 13 406 galaxies are classified as central galaxies in this way.

Figure 1 shows the distributions of stellar mass (left panel) and half light radius (right panel) for our samples. In the figure we use black lines for `Sample S0.55` and grey lines for `Sample S1.0`. In each case, the solid line is for the full sample, while the dashed and dotted lines are respectively for the central galaxy subsample and the satellite galaxy subsample. The satellite galaxies are those which are not classified as centrals. On average, galaxies in `Sample S1.0` are slightly more massive than those in `Sample 0.55`. This can be understood from the known positive correlation between mass and size (e.g. Shen et al. 2003). The right panel shows that our galaxies are only marginally resolved: the R50 is comparable to or even smaller than the PSF in most cases. As mentioned above, due to this limitation we choose to only consider a two-zone color and estimate the color gradient of a given galaxy by comparing the inner and outer colors. In this case, the measurements of both the two-zone color and the gradient should be reliable enough for our study.

3 RESULTS

3.1 Correlation of Color Gradient with Galaxy Properties

We begin by examining the correlations of the two-zone color $\Delta(u-r)$ and the color gradient $G_{\rm ur}$ with a variety of galaxy properties.

Figure 2 displays the distributions of both $\Delta(u-r)$ (left panel) and $G_{\rm ur}$ (right panel), for different samples. As in the previous figure, black lines are for `Sample S0.55` and grey lines for `Sample S1.0`. Solid lines in both panels are for the full sample. The $\Delta(u-r)$ distributions of the central and satellite galaxies in our sample are plotted with dashed and dotted lines respectively in the left panel, while the distributions of the passive and active SFGs are plotted in the dashed and dotted lines respectively in the right panel. We see that the different samples show quite similar distributions in the two-zone color, which are centered nearly at zero with a roughly symmetric distribution profile around the center. This suggests that, on one hand, the galaxies in our sample are flat on average in their color profile, and, on the other hand, the two colors span a wide range in $\Delta(u-r)$, ranging from ~ -1 up to ~ 1. Therefore, a large fraction of the sampled galaxies has either a negative color gradi-

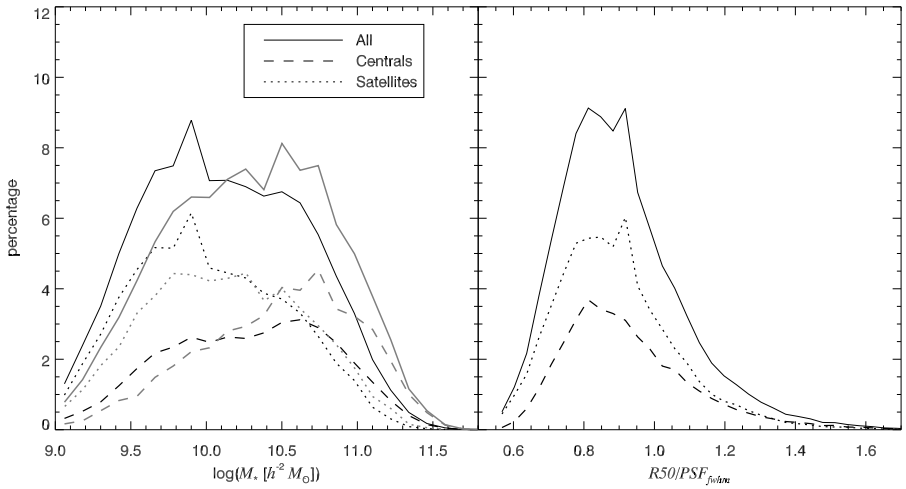

Fig. 1 Normalized distribution of stellar mass (*left panel*) and half light radius over $\mathrm{PSF}_{\mathrm{fwhm}}$ of our sample based on Equation (1) (*right panel*). We use *black lines* for `Sample S0.55` and *grey lines* for `Sample S1.0`. In each case, the *solid line* is for the full sample, while the *dashed* and *dotted lines* are respectively for the central galaxy subsample and the satellite galaxy subsample.

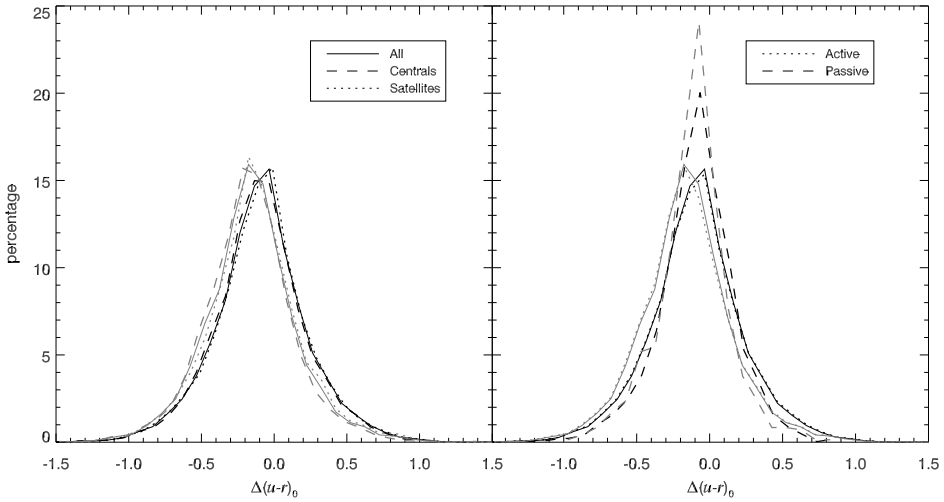

Fig. 2 Normalized $\Delta(u-r)$ distribution. We use *black lines* for `Sample S0.55` and *grey lines* for `Sample S1.0`. In each case, the *solid line* is for the full sample. The *dashed* and *dotted lines* are respectively for the central galaxy subsample and the satellite galaxy subsample in the left panel, while they are for passive and active subsamples in the right panel.

ent with a relatively red center, or a positive color gradient with a relatively blue center. In the next subsection, we will select the subsets of galaxies with "red cores" or "blue cores" and compare the properties of their host galaxies. In addition, the right panel of Figure 2 shows that passive galaxies present a narrower distribution than active galaxies, with a larger fraction of passive galaxies at $\Delta(u-r) \sim 0$.

Figure 3 displays the distribution of `Sample S0.55` on the plane of rest-frame two-zone color $\Delta(u-r)_0$ versus stellar mass (left panel), and the plane of color gradient G_{ur} versus stellar mass (right panel). We have corrected the incompleteness of our sample caused by the volume effect, by weighting each galaxy by $1/V_{\mathrm{max}}$, where V_{max} is the maximum volume over which the galaxy can be included in our sample. The diamonds in each panel represent the median $\Delta(u-r)_0$ or G_{ur} as a function of stellar mass, and the error bars indicate the 1σ scatter around the median relation. The lower panels display the distribution of the errors in $\Delta(u-r)_0$ and G_{ur} as a function of stellar mass. The errors are estimated based on the photometry errors and deviations from the best fitting SED model of the nearest bands in the rest frame.

Generally, we find both $\Delta(u-r)_0$ and G_{ur} to show very weak dependence on stellar mass, only slightly decreasing with increasing mass. The median value of both parameters is around zero at the lowest masses, thus showing no color gradient, and becomes negative

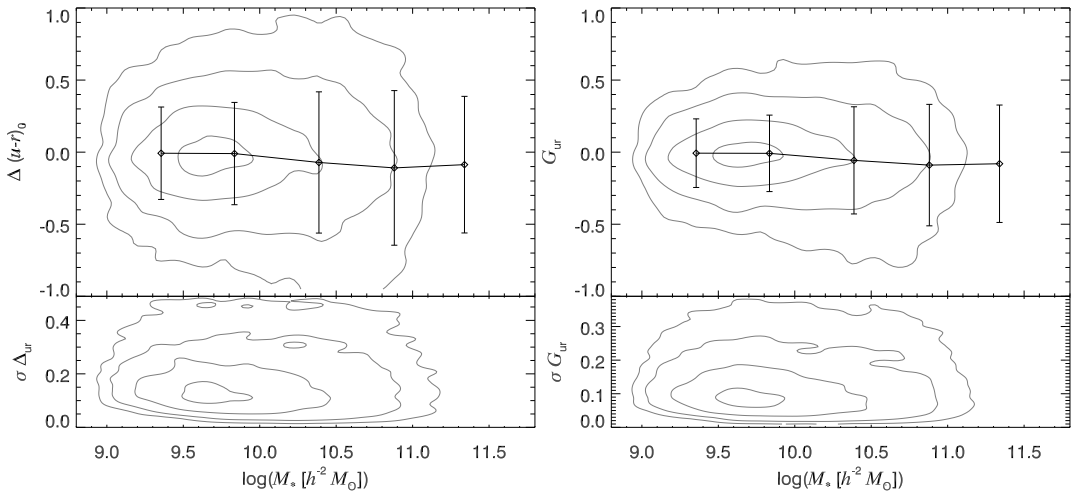

Fig. 3 Number density distributions of $\Delta(u-r)$ (*left panels*) and $G_{\rm ur}$ verses M_* (*right panels*) weighted by $1/V_{\rm max}$ for `Sample S0.55`. In each panel, the levels of the grey contours are 5%, 15%, 40% and 80% of the peak number density, and the larger number density corresponds to thicker contours in each panel. The medians and standard deviations are also plotted in *black lines* and error bars in the top panels. The bottom panels show the error distribution of $\Delta(u-r)$ (*left*) and $G_{\rm ur}$ (*right*).

at higher masses, reaching $\Delta(u-r)_0 \sim -0.2$ and $G_{\rm ur} \sim 0.1$ at the highest masses. This means that the most massive galaxies tend to have bluer colors in their outer regions when compared to the central region. This is very consistent with recent studies of integral field spectroscopy (IFS) on nearby galaxies, e.g. the Mapping Nearby Galaxies at Apache Point Observatory project (MaNGA; Bundy et al. 2015). For instance, Li et al. (2015) and Wang et al. (2018) investigated the gradient of recent SFH in MaNGA galaxies by jointly analyzing several spectral indices indicative of the SFH, finding that massive galaxies shutdown star formation from inside out. In that case, the central region gets quenched earlier, thus with older stellar population and redder color, than the outer region.

We show the comparison of $\nabla(g-i)$ at fixed $R50$ and M_* between `Sample S0.55` and low redshift results of Sloan Digital Sky Survey (SDSS; York et al. 2000) DR4 from Tortora et al. (2010) (hereafter `T10`) in Figure 4. Here we apply the color gradient definition from `T10` as $\nabla(g-i) = \Delta(g-i)/\log(\Delta R/R_{\rm eff})$. As we can see from both panels, $\nabla(g-i)$ measured in intermediate and low redshifts has similar trends with galaxy size and mass: $\nabla(g-i)$ of LTGs or active galaxies is anti-correlated with stellar mass and galaxy size; the median relation of ETGs or passive galaxies is flatter, especially at larger size or higher mass end. The gradients measured from our sample are smaller because of the contamination between the inner and outer regions due to the effect of PSF. The comparison implies that color gradients at intermediate and low redshifts have similar behaviors.

Next, we consider more properties of galaxies in Figure 5, where we show the correlation of $\Delta(u-r)$ with redshift, rest-frame colors $(u-r)$ and $(r-K)$, concentration index $R80/R50$, specific SFR (sSFR, SFR/M_*), half light radius ($R50$), B-band absolute magnitude (M_B), UBV parameter and B-band stellar mass-to-luminosity ratio (M_*/L_B). Here the UBV parameter is a combined color measured on the $U-B$ versus $B-V$ diagram following Krywult et al. (2017), by projecting the galaxy rest-frame $U-B$ and $B-V$ colors along the line that connects the density peaks of red and blue populations. The parameter is defined as

$$UBV = (B-V)\times\cos(\theta) - (U-B)\times\sin(\theta),$$

where θ is the slope of the connecting line on the diagram. As pointed out in Krywult et al. (2017), a combined color like UBV allows separation of the red/blue populations to be even more prominent than using a single color index.

As we can see from Figure 5, in most cases the median two-zone color shows weak/no dependence on galaxy properties. We see a marginal tendency for $\Delta(u-r)$ to decrease slowly with increasing global colors ($u-r$ and $r-K$), half-light size $R50$, luminosity (M_B) and mass-to-light ratio (M_*/L_B). Low-redshift studies (e.g. Liu et al. 2009) also find these correlations and these trends are all consistent with the dependence on stellar mass as found in the previous figure, because galaxies with high masses typically have higher luminosities (thus smaller M_B), redder colors (thus larger $(u-r)$ and $(r-K)$), larger sizes (thus larger $R50$) and larger mass

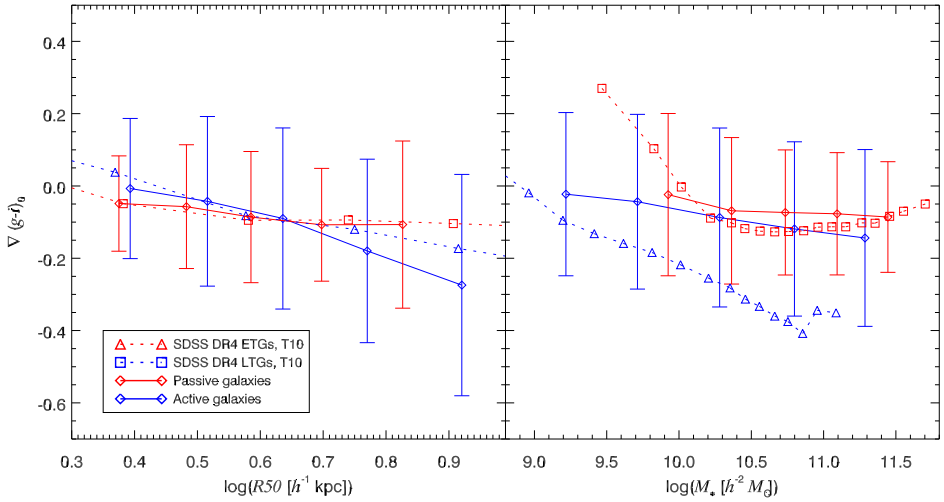

Fig. 4 Comparison of $\nabla(g-i)$ at fixed $R50$ and M_* between `Sample S0.55` and low redshift results of SDSS DR4 from Tortora et al. (2010). The *blue* (*red*) *diamonds* and error bars connected by *solid lines* show the $\nabla(g-i)$ of active (passive) galaxies from `Sample S0.55`, and *open blue* (*red*) *squares* (*triangles*) connected by *dotted lines* indicate $\nabla(g-i)$ of LTGs (ETGs). Results from low redshifts have similar error bar sizes, but they are not presented in the plot for clarity.

to light ratio. It is interesting that, although $\Delta(u-r)$ also slightly correlates with the combined color UBV, the correlation appears to be weaker than that with $u-r$ or $r-K$. This might suggest that the correlation with single color indices is not as strong as what we see, but rather is a result of the correlation of $\Delta(u-r)$ with stellar mass.

We conclude that the two-zone color (and color gradient) is anti-correlated with stellar mass, with negative color gradient (thus redder color in the inner region and bluer color in the outer region) at higher masses. On average, other properties of galaxies show weak or no independent correlations with the two-zone color.

3.2 "Red cores" versus "Blue cores"

Although in most cases our galaxy sample exhibits a nearly flat color gradient on average, individual galaxies span a wide range in the two-zone color and color gradient. It is interesting to examine the properties of those galaxies with either positive or negative gradients. This is the purpose of the current subsection.

Figure 6 displays the distribution of our galaxies (`Sample S0.55`) on the $\Delta(u-r)$ versus $\lg(M_*)$ diagram again. The diamonds and error bars show the median relation with 1σ scatter as depicted in Figure 3. Red and blue dots represent individual galaxies in our sample that fall outside the 1σ region of the median region. We define the galaxies plotted in red dots as "red core" galaxies and those in blue dots as "blue core" galaxies. By definition in this way, a "red core" galaxy has a relatively red color in its inner region compared to the outer region, while a "blue core" galaxy has a relatively blue color in the inner region. We ignore the galaxies within the 1σ region of the median relation and consider only the galaxies at the two ends in order to avoid contamination of the PSF effect on the classification. This selection gives rise to a sample of ∼5000 galaxies out of the `Sample S0.55` with either a red core or a blue core, and a sample of ∼1100 galaxies from `Sample S1.0`.

In Figure 7, we display the color distribution for the "red core" (red lines) and "blue core" galaxies (blue lines) using both `Sample S0.55` (solid lines) and `Sample S1.0` (dotted lines). For comparison, the results for the full samples are plotted in black lines. The left and right panels are for $r-K$ and $V-J$ colors respectively. Overall, all the samples show very similar distributions in both color indices. Galaxies with red cores are slightly redder on average than galaxies with blue cores, as indicated by the vertical short lines in both panels, with mean colors of $(r-K)\sim 0.85$ and $(V-J)\sim 1$ in red-core galaxies compared to $(r-K)\sim 0.75$ and $(V-J)\sim 0.95$ in blue-core galaxies.

In Figure 8, we further compare other properties between the red-core and blue-core galaxies. Each panel shows the median relation of a given property and galaxy stellar mass, plotted in red/blue symbols for the red-core and blue-core subsamples respectively. The error bars indicate the errors of the median property on the y-axis, quantified by Poisson errors but not the scatter of the sample around the median relation. The properties considered include surface mass density μ_*, rest-frame color

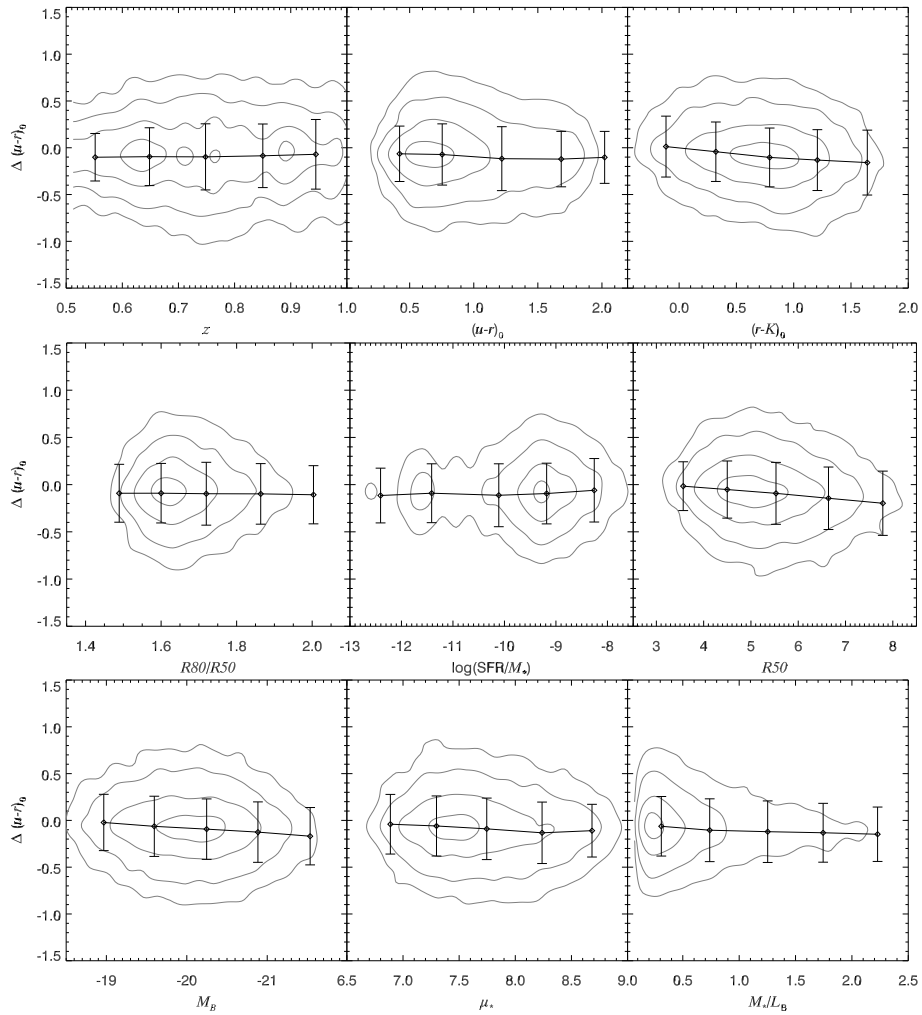

Fig. 5 Correlations between $\Delta(u-r)$ and a series of properties, which are redshift, rest-frame $(u-r)$ colors (ur) and (rK), concentration index R80/R50, sSFR (SFR/M_*), half light radius ($R50$), B-band absolute magnitude (M_B), combined color UBV and B-band stellar mass-to-luminosity ratio M_*/L_B. In each panel, the levels of the grey contours are 5%, 15%, 40% and 80% of the peak number density, and the larger number density corresponds to thicker contours in each panel. The medians and standard deviations are also plotted in *black lines* and error bars respectively.

$(r-K)_0$, the combined color UBV, the half-light radius $R50$, sSFR and ratio of total far-infrared (FIR) luminosity to UV luminosity (IRX), which is an indicator of dust attenuation.

Both the slightly redder global $r-K$ color in red-core galaxies and the null difference in the combined color UBV, as seen in the previous figure, are also seen in the current figure (see the upper panels). In addition, the figure shows that the two populations are identical in their median sSFR and this is true at all masses. The blue-core galaxies tend to be more dusty than the red-core population at intermediate masses ($M_* \sim 10^{10} - 10^{10.5}\,M_\odot$), but the difference is only marginal.

At fixed mass, the half-light size $R50$ presents a significant difference between the red- and blue-core galaxies, as can be seen from the leftmost panel in the lower row of Figure 8. Galaxies with red cores are larger than those with blue cores when stellar mass exceeds $\sim 10^{10}\,M_\odot$, and the effect becomes stronger with increasing stellar mass. For the most massive galaxies in our sample with $M_* > 10^{11}\,M_\odot$, $R50$ of the red-core galaxies is on average larger than that of the blue-core galaxies by about 20%. This means that the red-cored galaxies have lower surface stellar mass density than the blue-cored galaxies, as shown in the top-left panel. At the lowest masses ($M_* < 10^{9.5}\,M_\odot$), the two populations have similar sizes and the difference in $R50$ is no longer significant. Liu et al. (2009) investigated the color gradient of disk galaxies in SDSS and found that color gradients of disk galaxies correlate well with galaxy sur-

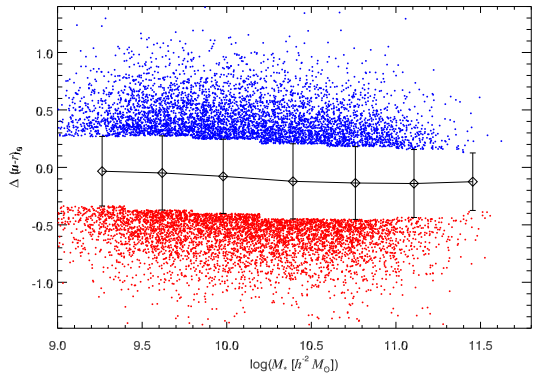

Fig. 6 $\Delta(u-r)$ vs. M_* distribution for `Sample S0.55`. The *diamonds* and error bars show the median relation with 1σ scatter. *Red* and *blue dots* represent individual galaxies in our sample that fall outside the 1σ region. The *red* and *blue dots* correspond to red core and blue core galaxies respectively in this work.

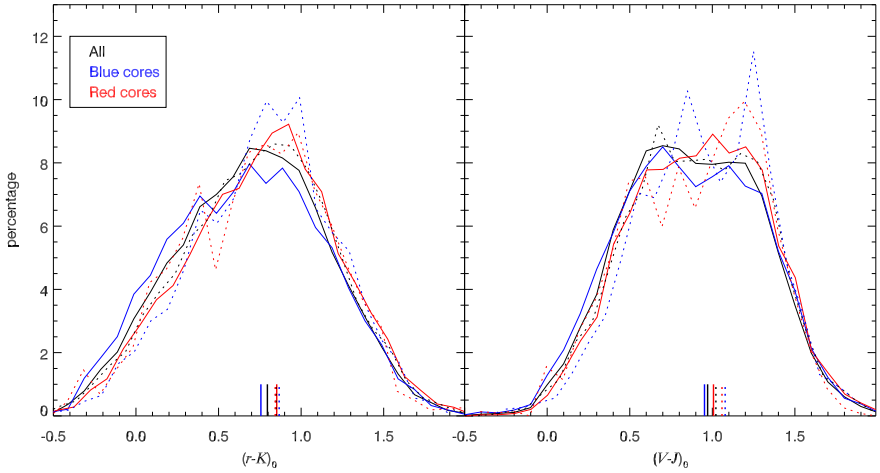

Fig. 7 Normalized $(r-K)_0$ (*left panel*) and $(V-J)_0$ (*right panel*) distribution of red and blue cores, as well as the full sample. In each case, we use *red*, *blue* and *black lines* for red cores, blue cores and full sample respectively. We employ *solid lines* for `Sample S0.55` and *dotted lines* for `Sample S1.0`, and the corresponding medians are plotted in the bottom region with *vertical short lines*.

face brightness, which correspond to surface mass density for a sample with a narrow redshift range. Our result here is consistent with their finding.

In Figure 9, we examine the fraction of red galaxies (left panel) and the fraction of central galaxies (right panel) as a function of stellar mass, for both the full sample (black symbols) and the red-/blue-cored galaxies separately (red and blue symbols). The error bars indicate the binomial distribution error of given stellar mass bin. Overall, both the red fraction and central fraction increase when one goes from low to high masses, as expected. The red fraction is constant at around zero at the lowest masses below $M_* \sim 10^{10}\,M_\odot$, before sharply increasing at higher masses, up to ∼55% at the highest masses for the full sample. It is interesting that the two populations of galaxies behave differently in this figure in the sense that the red-cored galaxies have smaller red fractions at given mass. The difference gets larger at higher masses: at the highest masses the red fraction of the red-cored population is $\sim 30\%$, compared to $\sim 50\%$ for the blue-cored population. This result indicates that the overall increase of red fraction with mass is dominated more by galaxies with blue cores, and that the structural parameters such as surface stellar mass density might be related to the star formation quenching process in galaxies.

The right panel of Figure 9 shows that the two populations of galaxies are similar in the mass dependence of the central fraction. The population of red-cored galaxies presents smaller central fractions at low masses ($M_* \lesssim 10^{10.5}\,M_\odot$). This suggests low-mass galaxies with red-cores are preferentially found as satellite galaxies of their host dark matter halos. At higher masses, the red-cored galaxies have a slightly higher central fraction

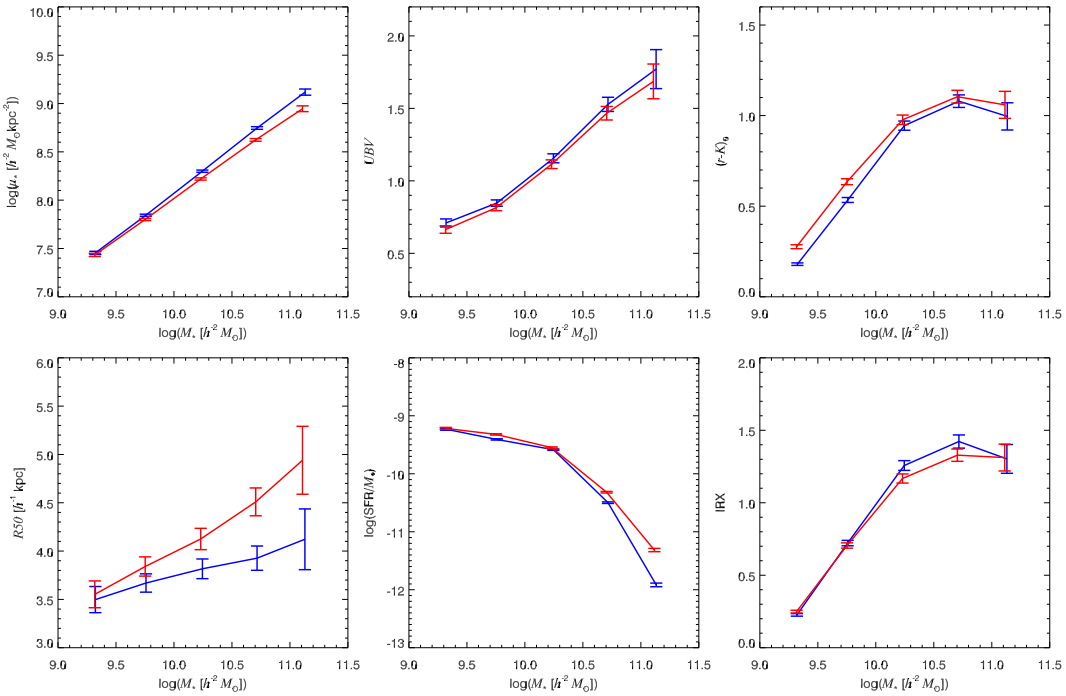

Fig. 8 Median relations of red-core and blue-core galaxies for given properties at fixed stellar mass. The properties are surface mass density μ_*, combined color UBV, rest-frame color $(r-K)_0$, half light radius ($R50$), sSFR (SFR/M_*) and ratio of total FIR luminosity to UV luminosity (IRX) versus stellar mass. *Red/blue* symbols correspond to the red-core and blue-core subsamples respectively, and the errors correspond to Poisson errors of each bin.

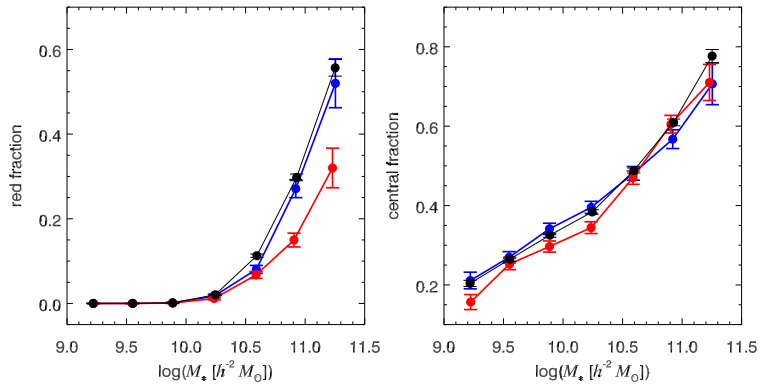

Fig. 9 Red fraction (*left panel*) and central fraction (*right panel*) versus galaxy stellar mass. In each case, we use *filled red circles* for red cores, *filled blue circles* for blue cores and *filled black circles* for the full sample. The error bars indicate errors of the binomial distribution for a given stellar mass.

than the blue-cored galaxies. Wang et al. (2010) found that optically selected brightest cluster galaxies in the local Universe tend to have redder NUV$-r$ colors in their centers than control galaxies. Our result here is along the same line as their finding.

4 SUMMARY

In this paper we present our attempt to statistically examine the color gradient in galaxies at intermediate redshifts. We use both the spectroscopic galaxy sample from the VIPERS project, which obtained spectroscopy for more than 90 000 galaxies at $0.5 < z < 1.0$, and the multi-band photometry from the VIPERS-MLS catalog which provides accurate photometry for the VIPERS galaxies in multiple bands in NUV, optical and NIR. We have selected a sample of 35 279 galaxies with reliable redshift measurements and relatively large sizes ($R50 > 0.55$ PSF) in order to have good spatial resolution. We estimated a variety of physical parameters by performing SED fitting to the multi-band photometry, including rest-frame luminosities in different bands, SFR

and stellar mass. We also measure the photometry for the inner and outer regions of each galaxy in our sample, thus obtaining a rest-frame two-zone color $\Delta(u-r)_0$ and a color gradient parameter $G_{\rm ur}$. We have examined the correlation of these two parameters with the global properties of galaxies, and compared the properties of the galaxies with red and blue cores.

Our conclusions can be summarized as follows:

- The two-zone color $\Delta(u-r)$ and color gradient $G_{\rm ur}$ are both anti-correlated with stellar mass, with negative color gradient (thus relatively red color in the inner region) at higher masses. Galaxy properties other than stellar mass show weak or no independent correlations with $\Delta(u-r)$ or $G_{\rm ur}$.
- Galaxies with red cores and galaxies with blue cores show similar distributions in most properties, and the half-light radius $R50$ and surface mass density μ_* are the only galaxy properties which show a significant difference between the two populations of galaxies. For galaxies more massive than $\sim 10^{10}\,M_\odot$, at fixed stellar mass, red-cored galaxies are larger, with the effect being larger at higher masses, and have smaller surface mass density.
- Red-cored galaxies show a lower red fraction than blue-cored galaxies at masses above $\sim 10^{10.5}\,M_\odot$, and lower central galaxy fraction at masses below $\sim 10^{10.5}\,M_\odot$.

The behaviors of the color gradient of our galaxies are similar to those of low-z galaxies, which have been extensively studied in the past few decades based on large redshift surveys such as the SDSS. This probably is not surprising, because violent processes like galaxy-galaxy mergers are believed to play important roles only at high redshifts (e.g. $z > 1$) and secular processes have been the driving processes for galaxy evolution since then. Therefore, it is highly expected to find the local galaxies behaving similarly at some level to galaxies at redshifts of $0.5 < z < 1$.

One interesting result from this work is the lower red fraction for the red-cored massive galaxies compared to the blue-cored galaxies of the same mass. This result may be understood in the picture of "inside-out" star formation quenching, as observed in the local galaxy population (e.g. Li et al. 2015; Wang et al. 2018). Based on the IFS of ~ 2000 nearby galaxies, these authors investigated the resolved map of recent SFH and suggested that, in massive galaxies with stellar mass above $\sim 10^{10}\,M_\odot$, star formation shutdown firstly occurs in the central region before extending to larger and larger radii. In this case, the central region would become red earlier than the outer region, and a galaxy at this stage would be classified as a red-cored galaxy following our definition. At a later stage when the galaxy is more evolved with larger area to be quenched, the galaxy would present less gradient in color and is more likely classified as a blue-cored galaxy. (The name "blue-core" does not really mean a blue center in this case.) Therefore, red-cored galaxies are actually less quenched than blue-cored galaxies, and this explains the lower red fraction of the red-core galaxy population in the left panel of Figure 9.

Another interesting result from our work is the larger size (thus lower surface mass density) of red-cored galaxies at fixed mass compared to blue-cored galaxies. As discussed above, red-cored galaxies are on average less quenched than blue-cored galaxies. Therefore, this result implies that the quenching status of a galaxy tends to relate with the stellar surface mass density: more quenched galaxies have higher densities. This is obvious and also consistent with studies of low-z galaxies, which show a bimodal distribution in surface mass density at given mass, with the high (low) density sub-population having a red (blue) global color. However, as shown in Wang et al. (2018), although the fraction of quenched galaxies is higher if their surface mass density is higher, the quenching process seems to be driven only by mass (or whatever physical processes are responsible for mass growth). Better data and more works are needed in order to better understand the quenching processes in galaxies with different redshifts. It is also important to examine the environment of our galaxies and study the potential effect of environment on different scales on the color gradient of galaxies at $0.5 < z < 1$. We will address this problem in a parallel paper using the same data.

Acknowledgements This work is supported by the National Key Basic Research Program of China (No. 2015CB857004) and the National Natural Science Foundation of China (Grant Nos. 11173045, 11233005, 11325314 and 11320101002). This paper uses data from the VIMOS Public Extragalactic Redshift Survey (VIPERS). VIPERS has been performed using the ESO Very Large Telescope, under the "Large Programme" 182.A-0886. The participating institutions and funding agencies are listed at *http://vipers.inaf.it/*. This paper is based on observations obtained with MegaPrime/MegaCam, a joint project of CFHT and CEA/IRFU, at the Canada-France-Hawaii Telescope (CFHT) which is operated by the National Research Council (NRC) of Canada, the Institut National des Science de l'Univers of the Centre National de la

Recherche Scientifique (CNRS) of France, and the University of Hawaii. This research makes use of the VIPERS-MLS database, operated at CeSAM/LAM, Marseille, France. This work is based in part on observations obtained with WIRCam, a joint project of CFHT, Taiwan, Korea, Canada and France. This work is also based in part on observations made with the *Galaxy Evolution Explorer* (*GALEX*). *GALEX* is a NASA Small Explorer, whose mission was developed in cooperation with the Centre National d'Etudes Spatiales (CNES) of France and the Korean Ministry of Science and Technology. *GALEX* is operated for NASA by the California Institute of Technology under NASA contract NAS5-98034. This work is based in part on data products produced at TERAPIX available at the Canadian Astronomy Data Centre as part of the Canada-France-Hawaii Telescope Legacy Survey, a collaborative project of NRC and CNRS. The TERAPIX team has performed the reduction of all the WIRCAM images and the preparation of the catalogs matched with the T0007 CFHTLS data release.

References

Arnouts, S., Le Floc'h, E., Chevallard, J., et al. 2013, A&A, 558, A67
Bertin, E., & Arnouts, S. 1996, A&AS, 117, 393
Bildfell, C., Hoekstra, H., Babul, A., & Mahdavi, A. 2008, MNRAS, 389, 1637
Boroson, T. A., Thompson, I. B., & Shectman, S. A. 1983, AJ, 88, 1707
Bruzual, G., & Charlot, S. 2003, MNRAS, 344, 1000
Bundy, K., Bershady, M. A., Law, D. R., et al. 2015, ApJ, 798, 7
Calzetti, D., Armus, L., Bohlin, R. C., et al. 2000, ApJ, 533, 682
Cibinel, A., Carollo, C. M., Lilly, S. J., et al. 2013, ApJ, 777, 116
Conseil, S., Vibert, D., Amouts, S., et al. 2011, in Astronomical Society of the Pacific Conference Series, 442, Astronomical Data Analysis Software and Systems XX, ed. I. N. Evans, A. Accomazzi, D. J. Mink, & A. H. Rots, 107
Cuillandre, J.-C. J., Withington, K., Hudelot, P., et al. 2012, in Proc. SPIE, 8448, Observatory Operations: Strategies, Processes, and Systems IV, 84480M
Daddi, E., Renzini, A., Pirzkal, N., et al. 2005, ApJ, 626, 680
Dale, D. A., Helou, G., Magdis, G. E., et al. 2014, ApJ, 784, 83
de Jong, R. S. 1996, A&A, 313, 377
Edwards, L. O. V., Hudson, M. J., Balogh, M. L., & Smith, R. J. 2007, MNRAS, 379, 100
Ferreras, I., Lisker, T., Carollo, C. M., Lilly, S. J., & Mobasher, B. 2005, ApJ, 635, 243
Ferreras, I., Lisker, T., Pasquali, A., Khochfar, S., & Kaviraj, S. 2009, MNRAS, 396, 1573
Gonzalez-Perez, V., Castander, F. J., & Kauffmann, G. 2011, MNRAS, 411, 1151
Guo, Y., Giavalisco, M., Cassata, P., et al. 2011, ApJ, 735, 18
Guzzo, L., Scodeggio, M., Garilli, B., et al. 2014, A&A, 566, A108
Ilbert, O., Arnouts, S., Le Floc'h, E., et al. 2015, A&A, 579, A2
Kim, K. O., & Ann, H. B. 1990, Journal of Korean Astronomical Society, 23, 43
Kormendy, J., & Djorgovski, S. 1989, ARA&A, 27, 235
Krywult, J., Tasca, L. A. M., Pollo, A., et al. 2017, A&A, 598, A120
Li, C., Wang, E., Lin, L., et al. 2015, ApJ, 804, 125
Liu, C.-Z., Shen, S.-Y., Shao, Z.-Y., et al. 2009, RAA (Research in Astronomy and Astrophysics), 9, 1119
Liu, F. S., Jiang, D., Guo, Y., et al. 2016, ApJ, 822, L25
Liu, F. S., Jiang, D., Faber, S. M., et al. 2017, ApJ, 844, L2
Maraston, C., Pforr, J., Renzini, A., et al. 2010, MNRAS, 407, 830
Martin, D. C., Fanson, J., Schiminovich, D., et al. 2005, ApJ, 619, L1
Menanteau, F., Jimenez, R., & Matteucci, F. 2001, ApJ, 562, L23
Michard, R. 2005, A&A, 441, 451
Moutard, T., Arnouts, S., Ilbert, O., et al. 2016a, A&A, 590, A102
Moutard, T., Arnouts, S., Ilbert, O., et al. 2016b, A&A, 590, A103
Noll, S., Burgarella, D., Giovannoli, E., et al. 2009, A&A, 507, 1793
Oke, J. B., & Gunn, J. E. 1983, ApJ, 266, 713
Papovich, C., Finkelstein, S. L., Ferguson, H. C., Lotz, J. M., & Giavalisco, M. 2011, MNRAS, 412, 1123
Salpeter, E. E. 1955, ApJ, 121, 161
Schlegel, D. J., Finkbeiner, D. P., & Davis, M. 1998, ApJ, 500, 525
Scodeggio, M., Guzzo, L., Garilli, B., et al. 2018, A&A, 609, A84
Shen, S., Mo, H. J., White, S. D. M., et al. 2003, MNRAS, 343, 978
Spolaor, M., Kobayashi, C., Forbes, D. A., Couch, W. J., & Hau, G. K. T. 2010, MNRAS, 408, 272
Suh, H., Jeong, H., Oh, K., et al. 2010, ApJS, 187, 374
Tortora, C., Napolitano, N. R., Cardone, V. F., et al. 2010, MNRAS, 407, 144
Wang, E., Li, C., Xiao, T., et al. 2018, ApJ, 856, 137
Wang, J., Overzier, R., Kauffmann, G., von der Linden, A., & Kong, X. 2010, MNRAS, 401, 433
York, D. G., Adelman, J., Anderson, Jr., J. E., et al. 2000, AJ, 120, 1579